Short Communication

A DFT Study on Application of Dual-Atom Fe$_2$/Phthalocyanine Catalyst for N$_2$ Reduction Reaction

L. Yang[*], *X. Ma, Y. Y. Xu, J. Y. Xu, Y. D. Song*[*]

School of Energy and Power Engineering, Jiangsu University of Science and Technology, 212003, Zhenjiang, Jiangsu, China
[*]E-mail: yljust18@163.com, songyindong@just.edu.cn

As the fundamental reactions, artificial ammonia synthesis via nitrogen reduction reaction (NRR) under mild environment is indispensable but challenging. In order to replace the commercial Ru catalyst, the development of the efficient catalyst with the abundant resource is of prominent significance. By density functional theory calculations, the NRR feasibility of dual transition metal doped phthalocyanine is systematically investigated wherein the Sc, Ti, V, Cr, Mn, Fe, Co, Ni, Cu, Zn and Mo are considered as the dopants. The results reveal that the activity is highly sensitive to the TM introduction wherein the phthalocyanine with Fe$_2$ dual-atom center encounters the minimal thermodynamic barrier with the value of 0.19 V. Furthermore, the strong binding strength between the Fe$_2$ and its surrounding enables the excellent stability against clustering. In addition, the inverted-volcano curve is established between the thermodynamic barrier and the adsorption energy of *NNH, due to the difficulty of the first protonation. From the Mulliken charge analysis, the electron transfer between Pc and the adsorbents is occurred through Fe$_2$N$_6$ moiety. Overall, this work opens up the design of the robust electrode material for N$_2$-to-NH$_3$ conversion.

Keywords: nitrogen fixation, dual-site catalysts, density functional theory

1. INTRODUCTION

The conversion of nitrogen into ammonia is a chemical cornerstone progress since ammonia is promising platform molecule for the future renewable energy infrastructure owing to its high energy density and carbon-free nature[1, 2]. Industrially, in order to split the steady triple-bond of nitrogen, the Haber-Bosch process is carried out at elevated temperatures and high pressures, leading to the enormous energy consumption[3, 4]. Inspired by the biological nitrogen fixation, the electrocatalytic nitrogen reduction reaction (NRR) is rising as a sustainable and economical strategy at ambient temperature in order to overcome the shortages of Haber-Bosch process[5]. However, the NRR

progress is limited by the lack of the highly efficient electrode. Therefore, a great challenge has been paved on the design and optimization of the electrocatalysts.

To conquer this issue, numerous efforts have been devoted to the two-dimensional single or dual atom catalysts (SACs or DACs) owing to its good electrical conductivity, ductility and stability. As previous reported, the NRR performance is originated from the combination of the given active center and the corresponding support. For instance, Mo doped BN monolayer possesses good NRR catalytic activity[6]. Subsequently, Du et al. developed B decorated g-C_3N_4 with ultralow overpotential for photocatalysis NRR[7]. In addition, Xiao et al. revealed that VN_3 decorated graphane improves the selectivity of the NRR[8]. Besides SACs, Chen et al. demonstrated that the Mn_2 anchored C_2N greatly enhanced the catalytic activity of NRR with respect to the monomers[9]. Similar results have been reported by the other groups[9, 10]. That is, the DACs benefit the inherent good reactivity due to the presence of the dual-atom center. The interesting performances of the DACs on NRR electrocatalysis raise our great concern.

Metal organic frameworks (MOFs), a rising class of highly ordered two dimensional materials, consisted by TM centers and organic groups. Due to high microporosity, structural variability and large specific surface, it has extensively adopted in gas adsorption and dissociation, batteries and catalysis. Especially, the unique characteristics of MOFs hold giant potential in electrocatalysis application, including carbon dioxide reduction reaction[11], hydrogen evolution reaction (HER)[12] as well as oxygen reduction/evolution reaction[13]. Relevantly, Du et al. illustrated a Mo-based MOF as electrode material for nitrogen fixation with ultralow overpotential of 0.18 V, indicating the feasibility in the NRR field[14]. The referred information drives us to explore the probability of the DACs in the framework of the MOFs.
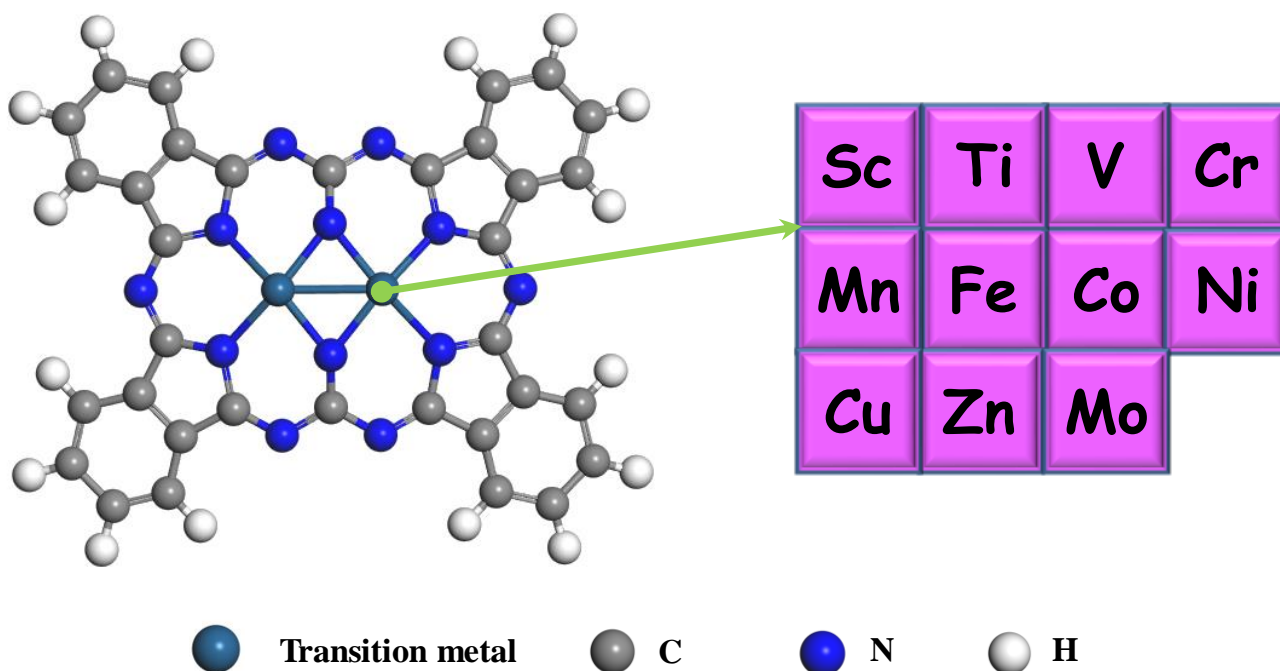

Figure 1. The atomic structure of TM_2 doped phthalocyanine (TM_2-Pc).

In the manuscript, the NRR performance of TM_2 doped phthalocyanine, termed as TM_2-Pc, is systematically investigated by density functional theory simulations. The atomic structure is schematically described in Figure 1. The stability of TM_2-Pc is analyzed by the binding energy E_b and bulk cohesive energy E_c. The stronger E_b indicates good resistance against clustering. Based on the information of the reaction energy, Fe_2-Pc possesses the lowest thermodynamic barrier with the value of 0.19 V along the enzymatic pathway, indicating the great promise for NRR application. Moreover, the N-NH* adsorption energy is identified as a simple parameter for material screening since the presence of the inverted-volcano between the barrier and N-NH* adsorption energy. From the Mulliken charge analysis, Fe_2N_6 moiety acts as a bridge for electron transfer between the Pc and NRR intermediates. The data provide the fundamental understanding the electrochemical activity of the functional phthalocyanine with TM_2 dopant.

2. COMPUTATIONAL METHOD

All calculations are performed within the DFT framework by $DMol^3$ code[15, 16]. The generalized gradient approximation with the Perdew–Burke–Ernzerhof (GGA–PBE) is adopted to describe exchange and correlation effects[17]. The DFT Semi-core Pseudopots (DSPP) core treat method is implemented for relativistic effects[18]. The double numerical atomic orbital augmented by a polarization function (DNP) is chosen as the basis set[15]. A smearing of 0.005 Ha (1 Ha = 27.21 eV) is applied to accelerate electronic convergence[19]. The convergence tolerances of energy, maximum force and displacement are 1.0×10^{-5} Ha, 0.002 Ha/Å and 0.005 Å, respectively[8]. The spin-unrestricted method is used for all calculations. A conductor-like screening model (COSMO) was used to simulate a H_2O solvent environment [20], where the dielectric constant is set as 78.54 for H_2O. In order to describe van der Waals (vdW) interactions, the Grimme scheme is adopted herein[21]. During the geometrical optimization, the systems are free to relax. To avoid the artificial interactions, the 15 Å-thick vacuum is added vertically to the Pc surfaces[13].

The adsorption energies E_{ads} are calculated by

$$E_{ads} = E_{system} - E_{catalyst} - E_m \qquad (1)$$

where E_{system}, $E_{catalyst}$ and E_m represent the total energy of the adsorption system, the catalyst and the adsorbates, respectively.

According to the computational hydrogen electrode (CHE)[22], the $\Delta E_{(U)}$ for elementary step at the potential U can be determined by

$$\Delta E_{(U)} = \Delta E - e\mathrm{U} \qquad (2)$$

where ΔE is energy from the DFT calculations, e is the electron and U is the bias voltage. $\Delta E_{(U)} < 0$ means an exothermic adsorption process, vise verse.

3. RESULTS AND DISCUSSION

The adsorption behavior of NRR intermediates is an important factor for reaction mechanism.

Furthermore, the optimized catalyst with the subtle adsorption affinity is the essential requirement according to the Sabatier principle. Therefore, the adsorption energies E_{ads} are evaluated and listed in Table 1. Definitely, the adsorption strength is highly sensitive to the TM_2 selection wherein the E_{ads} are ranged from -1.00 to 0.88 eV for *N_2, -3.05 to -0.06 eV for *N-NH, -3.65 to -0.33 eV for *HN-NH, -3.69 to -0.72 eV for *H_2N-NH, -4.25 to -1.59 eV for *H_2N-NH_2, -4.54 to -3.67 eV for *H_3N-NH_2 and -1.87 to -0.15 eV for *NH_3, respectively. Herein, the E_{ads}(*N_2) are summarized in Figure 2(a). As shown, the data are consistent with previous report[10], further supporting the reliability of our method. Furthermore, the positive values indicate the N_2 inaccessibility on the Cr_2-Pc, Mn_2-Pc and Co_2-Pc, being ruled out as NRR electrodes. Additionally, the early TM_2 provides the enhanced affinity with respect to the later counterparts, in line with the classical *d* band theory[23]. Subsequently, the competition between NRR and HER is considered in Figure 2(b). According to the previous studies[23, 24], the difference between the E_{ads}(*H) and E_{ads}(*N_2) is a simple descriptor to display the selectivity. The figure illustrates that Sc_2-Pc, Ti_2-Pc, V_2-Pc, Cr_2-Pc, Fe_2-Pc and Mo_2-Pc are NRR dominant. Combined the information of *N_2 adsorption and NRR selectivity, the five potential candidates are further considered for the activity discussion, involving Sc_2-Pc, Ti_2-Pc, V_2-Pc, Fe_2-Pc and Mo_2-Pc.
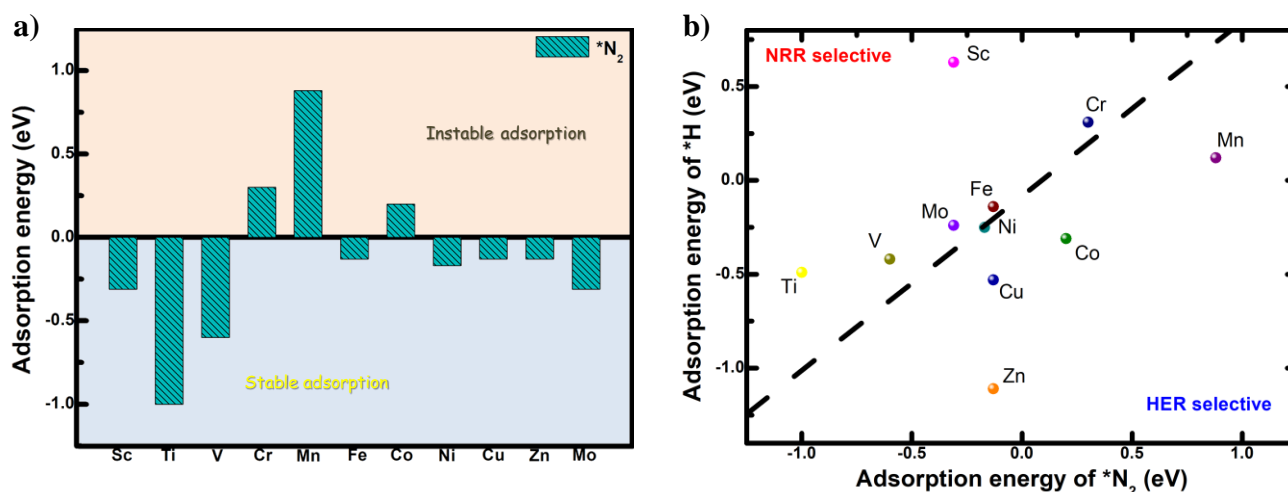

Figure 2. The adsorption energy (eV) of N_2 (a). The selectivity profiles for the NRR *vs* HER (b).

Table 1. Calculation of adsorption energy (eV) of intermediate products.

	Sc	Ti	V	Cr	Mn	Fe	Co	Ni	Cu	Zn	Mo
N_2	-0.31	-1.00	-0.60	0.30	0.88	-0.13	0.20	-0.17	-0.13	-0.13	-0.31
NNH	-1.36	-2.94	-2.80	-2.34	-1.88	-1.96	-1.70	-0.34	-0.06	-0.13	-3.05
HNNH	-1.70	-3.02	-3.25	-2.86	-2.13	-1.74	-1.20	-0.36	-0.33	-0.45	-3.65
H_2NNH	-2.06	-3.63	-3.69	-2.73	-1.99	-2.18	-2.01	-0.92	-0.72	-1.10	-3.42
H_2NNH_2	-3.45	-4.20	-4.25	-3.63	-3.12	-3.04	-2.86	-1.62	-1.59	-2.20	-3.83
H_3NNH_2	-3.69	-4.16	-4.54	-4.28	-3.85	-4.08	-4.41	-3.67	-3.76	-4.09	-4.47
H_3N	-1.35	-1.87	-1.84	-1.53	-0.83	-1.32	-1.45	-0.16	-0.15	-1.02	-1.68

Table 2. The reaction energy ΔE (eV) at the potential 0 V.

	Sc	Ti	V	Cr	Mn	Fe	Co	Ni	Cu	Zn	Mo
R_1	0.96	0.07	-0.18	-0.63	-0.45	0.19	0.11	1.84	2.08	2.02	-0.72
R_2	-0.87	-0.59	-0.97	-1.05	-0.77	-0.31	-0.02	-0.55	-0.79	-0.84	-1.04
R_3	-0.59	-0.86	-0.68	-0.10	-0.09	-0.67	-1.05	-0.79	-0.62	-0.90	-0.09
R_4	-1.39	-0.52	-0.56	-0.91	-1.13	-0.86	-0.72	-0.70	-0.87	-1.09	-0.41
R_5	0.83	1.08	0.78	0.52	0.35	0.03	-0.60	-0.98	-1.09	-0.81	0.44
R_6	-1.76	-1.81	-1.40	-1.44	-1.45	-1.25	-1.14	-0.59	-0.49	-1.04	-1.46
PDS	0.96	1.08	0.78	0.52	0.35	0.19	0.11	1.84	2.08	2.02	0.44
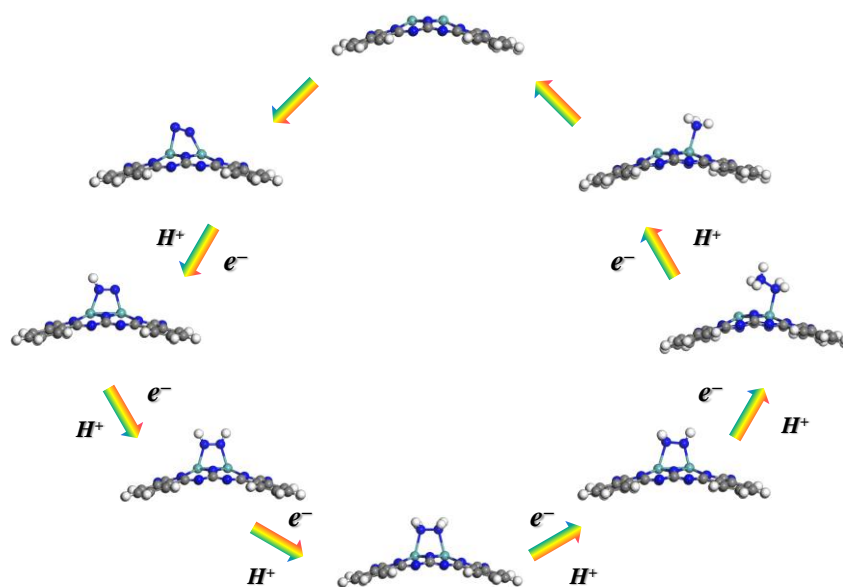
Figure 3. The adsorption configurations of the Fe_2-Pc.

To evaluate the NRR activity, the enzymatic pathway is considered due to the favor of the N_2 adsorption on side-on manner[8]. Specifically, the enzymatic mechanism is recommended due to then good ability to activate the noble N_2 molecule, as well revealed[6, 7, 10, 25]. The reaction energy changes (ΔE) of the elementary steps are tabulated in Table 2 wherein the positive value implies the reaction is thermodynamically limited meanwhile the negative one means its spontaneous feature. Figure 3 describes the NRR intermediates adsorption configurations of Fe_2-Pc under the enzymatic pathway as an illustration, wherein the two N atoms are hydrogenated by the proton-electron pairs alternately. Figure 4(a-e) presents the reaction energy profiles. Taken Fe_2-Pc in Figure 4(d) as an example, the energetically uphill of the *N-NH formation and *NH_2-NH_3 is observed with the ΔE of 0.19 and 0.03 eV meanwhile the rest steps are featured with exothermic characteristic where the corresponding ΔE are -0.31, -0.67, -0.86 and -1.25 eV, respectively. With the aid of the solution, the *NH_3 desorption is not a problem[26, 27]. Therefore, the potential-determining step (PDS) is the first protonation with the ΔE of 0.19 eV. Following the similar analysis[6, 8], the thermodynamic barriers of TM_2-Pc are summarized in Figure 4(f). Therein, the ΔE of PDS is ordered by Ti_2(1.08 eV) > Sc_2(0.96 eV) > V_2(0.78 eV) > Mo_2(0.44 eV) > Fe_2(0.19 eV), clearly supporting the dramatic influence of TM_2

dopant on the activity. In comparison with Ru(0001)[28], the heteroatoms of Fe_2, Mo_2 and V_2 exhibit the outstanding activity toward NRR, being promising alternatives. Furthermore, Figure 4(g) provides the correlation between the ΔE of PDS and the adsorption energy of E_{ads}(*N-NH)[28], where a classical inverted-volcano curve is observed with the vertex location of the Fe_2-Pc. The merged relationship reveals the feasibility of the simple parameter E_{ads}(*N-NH) for material screening process.

Figure 4. The reaction energy (eV) profiles for NRR via enzymatic pathway (a-e). The PDOS of Fe_2-*d* and coordination N-*p* orbitals (f). The binding energy E_b (eV) and bulk cohesive energy E_c (eV) (g). The thermodynamic barriers (eV) of PDS for NRR (h). The relationship between the PDS (eV) and the adsorption energy (eV) of *NNH (i).

Besides the activity, the stability of the aforementioned TM_2 is considered by the binding energy E_b between the TM_2 atoms and Pc monolayer. Figure 4(h) demonstrates that the E_b is enormously changed. The strength is ordered by Sc_2(-10.54 eV) > Ti_2(-10.19 eV) > V_2(-8.98 eV) > Fe_2(-8.65 eV) > Mo_2(-8.43 eV). Therein, the bulk cohesive energy E_c is added for comparative analysis. As depicted, all E_b are significantly exceeded E_c, indicating good stability against the aggregations. That is, the TM_2 anchoring is firmed enough during the experimental synthesis[29]. In order to reveal the physical origin of the stability, the electron structure analysis of Fe_2-Pc is further

discussed due to the similarity among TM_2-Pc. The partial density of state (PDOS) is given Figure 4(i). Obviously, the *pd* hybridization between the Fe_2 and the surrounding N is contributed to the strong interaction, in line with the results of Zhou et al.[25]. Overall, the excellent activity and good stability enables the Fe_2-Pc application in the N_2-to-NH_3 conversion.
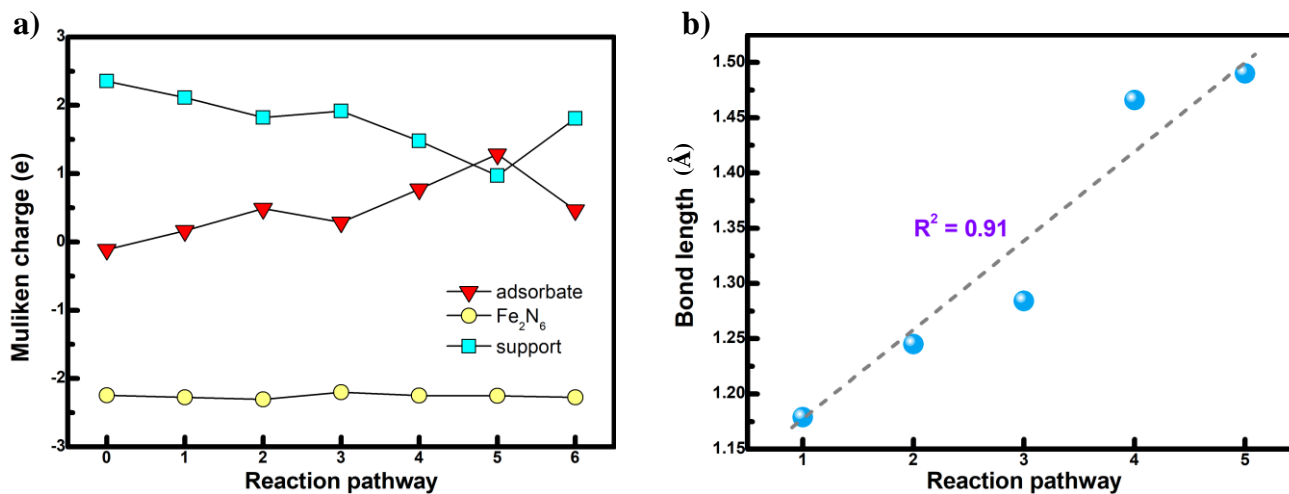

Figure 5. The Muliken charge analysis for variations of the three moieties (a). The N-N bond length change in NRR along the enzymatic pathway (b).

Generally, the orbital coupling ensures the electron transfer between the NRR intermediates and the electrode materials, especially for the catalysts with the TM_2 dopants[8, 23, 30]. To uncover the superior performance of Fe_2-Pc, the electron transfer between the Fe_2-Pc and NRR intermediates are analyzed and the corresponding Muliken charges are shown in Figure 5(a). As shown, the charge of Fe_2N_6 is negligibly changed during the consecutive protonations. Plausibly, it serves as a bridge for charge transfer between the adsorbent and the substrate, in consistent with previous reports[6]. Besides, the N-N bond lengths of the NRR intermediates are monitored in Figure 5(b). Therein, the linear stretch is observed during the reduction process. That is, the H attachments activate the inert N-N bonds, leading to the possibility of the N_2-to-NH_3 conversion under the mild condition. Overall, our results provide the Fe_2-Pc as good candidate for the future experimental verification.

4. CONCLUSIONS

In summary, the feasibility of TM_2-Pc as NRR electrode is systematically investigated by density functional theory calculations. The energy profiles reveal that the Fe_2-Pc exhibits the lowest thermodynamic barrier via the enzymatic pathway, being potential alternatives to the commercial Ru material. Additionally, the presence of the inverted-volcano relationship between the thermodynamic barrier and the adsorption energy of *N-NH indicates the importance of the first protonation. The activation of the NRR intermediates is ascribed to the electron transfer between the Pc and NRR intermediates via the Fe_2N_6 moiety. Furthermore, the Fe_2-Pc possesses good stability against

clustering, being originated from the *pd* orbital coupling. Foremost, our results highlight the robustness of the Fe2-Pc as the novel NRR electrode, providing the guidance for the material design. Besides, no attempts should be carried out, focused on Cr2-Pc, Mn2-Pc, Co2-Pc, Ni2-Pc, Cu2-Pc and Zn2-Pc due to the inaccessibility of the N2 molecules or the competitive HER side reaction. Furthermore, Sc2-Pc and Ti2-Pc are ruled out due to the inferior NRR activity.

CONFLICTS OF INTEREST
There are no conflicts to declare.

References

1. K. Nakajima, H. Toda, K. Sakata, Y. Nishibayashi, *Nat. Chem.*, 11 (2019) 702.
2. W. Qiu, X.Y. Xie, J. Qiu, W.H. Fang, R. Liang, X. Ren, X. Ji, G. Cui, A.M. Asiri, G. Cui, B. Tang, X. Sun, *Nat. Commun.*, 9 (2018) 3485.
3. G. Soloveichik, *Nat. Catal.*, 2 (2019) 377.
4. B.H.R. Suryanto, H.-L. Du, D. Wang, J. Chen, A.N. Simonov, D.R. MacFarlane, *Nat. Catal.*, 2 (2019) 290.
5. P. Wang, F. Chang, W. Gao, J. Guo, G. Wu, T. He, P. Chen, *Nat. Chem.*, 9 (2016) 64.
6. J. Zhao, Z. Chen, *J. Am. Chem. Soc.*, 139 (2017) 12480.
7. C. Ling, X. Niu, Q. Li, A. Du, J. Wang, *J. Am. Chem. Soc.*, 140 (2018) 14161.
8. B. B. Xiao, L. Yang, L.B. Yu, E.H. Song, Q. Jiang, *Appl. Surf. Sci.*, 513 (2020) 145855.
9. Z.W. Chen, J.M. Yan, Q. Jiang, *Small Methods*, 3 (2018) 1800291.
10. X. Guo, J. Gu, S. Lin, S. Zhang, Z. Chen, S. Huang, *J. Am. Chem. Soc.*, 142 (2020) 5709.
11. Z. Ma, D. Wu, X. Han, H. Wang, L. Zhang, Z. Gao, F. Xu, K. Jiang, *J. CO₂ Util.*, 32 (2019) 251.
12. Y. Wang, Y. Pan, L. Zhu, H. Yu, B. Duan, R. Wang, Z. Zhang, S. Qiu, *Carbon*, 146 (2019) 671.
13. B.B. Xiao, H.Y. Liu, X.B. Jiang, Z.D. Yu, Q. Jiang, *RSC Adv.*, 7 (2017) 54332.
14. Q. Cui, G. Qin, W. Wang, G. K.Rangaswamy, A. Du, Q. Sun, *J. Mater. Chem. A*, 7 (2019) 14510.
15. B. Delley, *J. Chem. Phys.*, 92 (1990) 508.
16. B. Delley, *J. Chem. Phys.*, 113 (2000) 7756.
17. B. PerdewJP, ErnzerhofM, *Phys. Rev. Lett.*, 77 (1996) 3865.
18. B. Delley, *Phys. Rev. B,* 66 (2002) 155125.
19. B. B. Xiao, H. Liu, L. Yang, E. Song, X. Jiang, Q. Jiang, *ACS Appl. Energy Mater.*, 3 (2019) 260.
20. T. Todorova, B. Delley, *Mol. Simulat.*, 34 (2008) 1013.
21. B. B. Xiao, X.Y. Lang, Q. Jiang, *RSC Adv.*, 4 (2014) 28400.
22. J.K. Nørskov, J. Rossmeisl, A. Logadottir, L. Lindqvist, J.R. Kitchin, T. Bligaard, H. Jonsson, *J. Phys. Chem. B*, 108 (2004) 17886.
23. C. Ling, Y. Ouyang, Q. Li, X. Bai, X. Mao, A. Du, J. Wang, *Small Methods*, 3 (2018) 1800376.
24. L. Li, B. Li, Q. Guo, B. Li, *J. Phys. Chem. C*, 123 (2019) 14501.
25. H.Y. Zhou, J.C. Li, Z. Wen, Q. Jiang, *Phys. Chem. Chem. Phys.*, 21 (2019) 14583.
26. Y. C. Hao, Y. Guo, L.W. Chen, M. Shu, X.-Y. Wang, T.-A. Bu, W.Y. Gao, N. Zhang, X. Su, X. Feng, J.W. Zhou, B. Wang, C.W. Hu, A.X. Yin, R. Si, Y.W. Zhang, C.H. Yan, *Nat. Catal.*, 2 (2019) 448.
27. C. Liu, Q. Li, C. Wu, J. Zhang, Y. Jin, D.R. MacFarlane, C. Sun, *J. Am. Chem. Soc.*, 141 (2019) 2884.

28. E. Skulason, T. Bligaard, S. Gudmundsdottir, F. Studt, J. Rossmeisl, F. Abild-Pedersen, T. Vegge, H. Jonsson, J.K. Norskov, *Phys. Chem. Chem. Phys.*, 14 (2012) 1235.
29. O. Matsushita, V.M. Derkacheva, A. Muranaka, S. Shimizu, M. Uchiyama, E.A. Luk'yanets, N. Kobayashi, *J. Am. Chem. Soc.*, 134 (2012) 3411.
30. L. Li, X. Wang, H. Guo, G. Yao, H. Yu, Z. Tian, B. Li, L. Chen, *Small Methods*, 3 (2019) 1900337